Improvement of LSM15-CGO10 electrodes for electrochemical removal of NOx by KNO3 and MnOx impregnation

Traulsen, Marie Lund; Kammer Hansen, Kent

Published in:
Journal of The Electrochemical Society

Link to article, DOI:
10.1149/2.086112jes

Publication date:
2011

Improvement of LSM15-CGO10 electrodes for electrochemical removal of NO_x by KNO_3 and MnO_x impregnation

M. L. Traulsen* K. Kammer Hansen

Fuel Cells and Solid State Chemistry Division, Risø National Laboratory for Sustainable Energy, Technical University of Denmark, DK-4000 Roskilde, Denmark

Abstract

LSM15-CGO10 ($La_{0.85}Sr_{0.15}MnO_3$-$Ce_{0.90}Gd_{0.1}O_{1.95}$) electrodes were impregnated with either KNO_3 or MnO_x, and the effect of the impregnations on the activity in NO containing atmospheres was investigated by electrochemical impedance spectroscopy and cyclic voltammetry. The electrodes were tested in 1000 ppm NO, 10% O_2 and 1000 ppm NO + 10% O_2 in the temperature range 300-500 °C and the electrodes were investigated by scanning electron microscopy before and after testing. At 400-450 °C a NO_x-storage process was observed on the KNO_3-impregnated electrodes, this process appeared to be dependent on preceding catalytically formation of NO_2. Despite a marked difference in the microstructure of the impregnated KNO_3 and MnO_x, both impregnations caused a significant reduction in the polarization resistance of the electrodes, due to a general decrease in resistance of all the identified electrode processes. The effect of the impregnation was strongest at low temperatures, likely because the microstructure of the impregnated compounds changed at higher temperatures. Scanning electron microscopy images revealed a significant change in the microstructure of the impregnated samples after the test.

* E-mail: matr@risoe.dtu.dk

Introduction

Air pollution from road traffic has due to the harmful effects on human health and environment got more and more attention during the last decades. In order to reduce air pollution, restrictions has been imposed on the emissions from vehicles, which on European level has been done by the introduction of the Euro I-VI standards. These standards impose increasing restrictions on the emission of CO, NO_x, hydrocarbons and particulate matter (1).

The increased restrictions on NO_x emissions are adopted, as NO_x has a negative impact on the respiratory system, increase the formation of ozone at ground level, cause formation of acid rain and also act as green house gas (2). To reduce the NO_x emission from vehicles several technologies have been developed, for NO_x-removal under lean conditions (i.e. in excess of oxygen) the three most known technologies are selective catalytic reduction with urea (urea-SCR), selective catalytic reduction with hydrocarbons (HC-SCR) and the NO_x-storage and reduction (NSR) catalyst (3).

An alternative way to remove NO_x under lean conditions is the electrochemical removal of NO_x, which was first suggested by Pancharatnam et al. (4). Since then several investigations has been made of electrochemical removal of NO_x (5-10). A general challenge in electrochemical removal of NO_x is to find electrodes, which both have a sufficient activity and show a high selectivity for NO_x reduction compared to reduction of O_2 (11). For this reason the aim in this work is to investigate if the activity and selectivity of LSM15-CGO10 electrodes towards NO_x can be improved by impregnating the electrodes with either KNO_3 or MnO_x.

KNO_3 is chosen for the impregnation, since K_2O/KNO_3 has shown potential as a NO_x-storage compound in nitrogen storage and reduction catalysts (12)(13)(14)(15), and for this reason is expected to improve selectivity and activity for NO_x reduction on the LSM15-CGO10 electrodes.

Just as KNO_3, MnO_x is also reported to have capability to store NO_x (16) and may for the same reasons improve the NO_x reduction selectivity and activity. Moreover, impregnated MnO_x may increase the general activity of the LSM/CGO electrode, as nano-sized MnO_x-particles may extend the triple-phase-boundary, and an extension of the triple-phase boundary in the literature is considered to be one of the important effects of electrode impregnation (17-19) . An increased activity with impregnation with MnO_x is expected, since Mn can exist in a number of oxidation states, and for this reason is the redox active center in perovskites used for redox catalysis (20) and also has been proven to affect the oxygen reduction reaction on electrodes (21).

In the present work symmetric cells with LSM15-CGO10 ($(La_{0.85}Sr_{0.15})_{0.99}MnO_{3+\delta}$-$Ce_{0.9}Gd_{0.1}O_{1.95}$) composite electrodes were prepared. LSM was chosen for this work due to the good stability of this perovskite compared to other perovskites like $La_{1-x}Sr_xFe_{1-y}Co_yO_3$ and $Ba_{1-x}Sr_xFe_{1-y}Co_yO_3$, eventhough these have a higher activity in the investigated temperature range (22). The cells were after the preparation divided into three groups and treated in three different ways: one group was impregnated with KNO_3, one group was impregnated with MnO and one group was left without any impregnation. The cells were following tested with electrochemical impedance spectroscopy and cyclic voltammetry. In addition to this cells from each of the three groups were investigated by scanning electron microscopy before and after testing.

Conductivity of KNO_3 and MnO_x compared to electrode materials

A point which must be considered is the conductivity of the impregnated materials, as an impregnated phase with conductivity much higher than the electrode materials could significantly alter the current distribution in the electrode. In the temperature range 350 °C – 500 °C the conductivity of KNO_3 increases from 0.669 S/cm to 1.094 S/cm (23). No information has so far been found concerning the conductivity of MnO_x at 300 °C – 500 °C, but MnO_2 is reported to have electronic conductivities in the range $5x10^{-7}$-$3x10^{-3}$ S/cm^2 at room temperature, the large range of the conductivities being due to a strong dependence on the crystallographic form of MnO_2

(24). Since MnO_2 is a semiconductor the conductivity will increase with increasing temperature. The electronic conductivity of LSM16/LSM20 is reported to be in the range 90-110 S/cm at 300-600 °C (25) (26) and for CGO10 the total conductivity at 500 °C is 0.005 S/cm (27){{233 Wang,S.R. 2000}}(27){{233 Wang,S.R. 2000}}(28)(25)(26). By comparing the conductivities of the impregnated compounds to the conductivities of the electrode materials it is clear the highest electronic conductivity will be found in the LSM15. For this reason the current distribution in the electrode is not expected to change due to the introduction of an "easier" current pathway in the electrode by the impregnation.

Experimental

Cell preparation

The LSM15 used for the electrodes was prepared by the glycine-nitrate combustion synthesis (28) with a molar ratio of 0.548 glycin/nitrate. The nitrates used for the synthesis were all from Alfa Aesar. The LSM was synthesized as $(La_{0.85}Sr_{0.15})_{0.99}MnO_3$, i.e. as being slightly deficient on the A-site. After the synthesis the LSM powder was calcined at 1000 °C for 6 hours, and subsequent the phase-purity of the powder was confirmed by XRD on a theta/theta Stoe diffractometer. The CGO10 powder used for the electrodes was supplied by Rhodia and had a BET area of 7.29 m^2/g.

The symmetric cells were manufactured by screen-printing a terpineol based LSM15-CGO10 paste on 200 µm thick CGO10 tapes from Kerafol. The ratio between LSM15 and the CGO10 in the screen-printing paste was 50wt% LSM15/50 wt% CGO10, and before mixing d50 was ≈1 µm for LSM15 and ≈0.5 µm for CGO10. After screen-printing the 50 x 50 mm^2 cells were sintered at 1050 °C for 2 h. The cells were after the sintering cut into small 6 x 6 mm^2 cells with a diamond toll. Finally a gold current collector was applied on the cells by painting the cells with a gold paste containing 20 wt% graphite. The cells were then heated to 800 °C in order

to burn away the graphite, leaving behind a porous, electronic conductive gold current collector on top of the electrodes.

For the impregnation with KNO_3 an aqueous solution containing 1.7 M KNO_3 and Triton-X45 surfactant was prepared. The concentration of Triton-X45 was 1 wt% with respect to the water. For the impregnation with $Mn(NO_3)_x$ a purely aqueous solution with 1.7 M $Mn(NO_3)_x$ was used. The impregnation was made by soaking the cells in the impregnation solution in a small beaker, which was placed in a vacuum chamber. The vacuum chamber was for less than a minute evacuated to a pressure below 0.1 mbar. After the impregnation the cells were heated in a furnace to 350 °C for one hour in order to:

1) Decompose the Triton-X45
2) Decompose the $Mn(NO_3)_x$ into MnO_x (29).

In addition to this the KNO_3 would melt during the heat treatment (mp(KNO_3)=334 °C (30)), and for this reason probably redistribute in the electrode. The impregnation procedure just described was repeated twice for both the KNO_3 and the $Mn(NO_3)_x$ impregnation.

Electrochemical characterization

For the electrochemical cell testing a four sample set-up was used in which each of the four cells was fixed between two gold meshes, which also acted as current collectors. The set-up was placed in a furnace, sealed and attached to the gas supply system. Before the set-up was heated a leak test was made.

During the cell test electrochemical impedance spectra (EIS) and cyclic voltammograms (CVs) were recorded in each of the three atmospheres: (1)1000 ppm NO in Ar, (2) 10% O_2 in Ar and (3) 1000 ppm NO + 10% O_2 with balance Ar. These concentrations of NO and O_2 were chosen as they resemble the concentrations which may be found in the exhaust from a diesel car (31). The EIS and CVs were recorded in the temperature range 300-

500 °C, as this is the temperature range expected for diesel car exhaust (32). The measurements were made with 50° intervals, starting from 300 °C and going to higher temperatures. At 500 °C flow variations were made by changing the flow from 100 ml/min to 50 ml/min in all three atmospheres. In addition to this variations in the NO concentration and O_2 concentration were made, but only for the cells without impregnation. After the measurements at 500 °C the temperature was decreased to 300 °C, and EIS were recorded once again in 1000 ppm NO + 10% O_2 to estimate the change during the cell test, before the furnace finally was cooled down. In general the EIS were recorded in the frequency range 1 MHz-0.0008 Hz with 6 points pr. decade and 36 mV rms amplitude, a few spectra were however recorded with a slightly different low frequency limit. The cyclic voltammograms were recorded between the voltage limits ±1V with scan rate 10 mV/s, step size 5 mV and 4 scans recorded for each measurement. Both the EIS and CV were recorded with a Gamry Reference 600 potentiostat.

It should be noted only in the test on LSM15-CGO10 cells without impregnation 4 cells were subjected to electrochemical cell testing (EIS and CVs), whereas in the two tests on impregnated cells only 3 cells were tested in each test. The fourth cell in the set-up in these two tests was not subjected to the electrochemical cell testing but experienced the exactly same temperature profile as the three electrochemically tested cells, and was later investigated in the scanning electron microscopy to observe the effect of the temperature on the microstructure.

Scanning Electron Microscopy

Tested and non-tested cells were investigated in a Zeiss Supra 35 scanning electron microscope. In order to be able to observe structures smaller than 200 nm, the cells were broken manually and the cross-section was investigated directly in the microscope without application of any coating. In order to ensure a high resolution most of the images were recorded with the in-lens detector and low accelerating voltage (3kV).

Results

Impregnation

The cells were weighed before and after impregnation to determine the impregnation load on the tested cells. For the cells impregnated with KNO_3 the final load was 0.3 ±0.1 wt% for three of the cells, whereas the last cell apparently lost weight during the impregnation. For the cells impregnated with MnO_x the final load was 0.5 ±0.2 wt%.

Cyclic voltammetry

For the 3-4 cells tested in each test good reproducibility is observed for cyclic voltammograms recorded at the same conditions within each test, both with respect to shape of the cyclic voltammogram and current densities. A general feature of the cyclic voltammograms recorded on both blank and impregnated cells is their shape depend on the atmosphere as illustrated in Figure 1 for the blank cells. Clear peaks were only observed on the CVs recorded in 1000 ppm NO at 400 and 450 °C on the KNO_3 impregnated sample, see Figure 2 where a comparison is made to a CV recorded on one of the blank cells.

From the cyclic voltammograms recorded in 1000 ppm NO +10% O_2 the current densities at 0.9 V was found for the three tests, the result is shown in Table 1; where the stated values are the averages from the 3-4 tested cells at both negative and positive polarisation. As the result for one of the cells impregnated with MnO_x deviates from the two other cells the values are stated separately in Table 1. In general the largest current densities are observed for impregnated samples, with the difference between the impregnated and the blank samples being most pronounced at low temperatures.

Fitting procedure

For fitting of the impedance spectra the program ZView 2, version 3.1c was used (33). An equivalent circuit was used which contained a serial resistance R_s and a number of RQ subcircuits, where a resistance (R) is in parallel with a constant phase element (Q). The admittance of the constant phase element may be written as (34)

$$Y = Y_0 (j\omega)^n$$

- where *Y* is the admittance, Y_0 is the amplitude of the constant phase element admittance, *j* is the imaginary number, *ω* is the angular frequency and *n* is the frequency exponent of the constant phase element. For the physical interpretation of the constant phase element, the near-equivalent capacitance (C_ω) was calculated according to the formula (35)

$$C_\omega = R^{(1-n)n} Y_0^{1/n}$$

All impedance spectra were fitted with one serial resistance and between 2 and 4 RQ-subcircuits. The fitting process consisted of two sessions: During the first session all the resistances and parameters for the constant phase elements were allowed to adjust during the fitting of a total number of at least 40 impedance spectra for each test. After this first session identical processes were identified by comparing the characteristic frequencies, C_ω and the n-values, and the average n-value was calculated for each of the identified processes. During the second session the impedance spectra were fitted once again, with the n-values fixed at the average values.

Conductivity

The average serial resistance of the cells was found for each test and converted to conductivities. The conductivities are stated in Figure 3 together with literature data for the conductivity of CGO calculated from the results found by Omar et al. 2009 (36).

In general fairly good agreement is achieved between conductivities of the blank cells and the KNO_3-impregnated cells compared to the conductivity of CGO reported in the literature, but especially at higher temperatures the conductivity of the blank sample is higher. The conductivity of the MnO_x-impregnated samples follow the conductivity of the other samples until 400 °C, whereafter the conductivity start to decrease even though the temperature increases.

Polarisation resistance

When comparing the size of the polarisation resistances between the three tests, see Table **2**, the polarisation resistance of both the impregnated samples is below the polarisation resistance of the blank samples in the temperature range 300-450 °C. At 500 °C the impregnated samples still have a lower polarisation resistance compared to the blank samples in 1000 ppm NO, but in 10% O_2 and 1000 ppm NO + 10% O_2 the polarisation resistance is either equal to or slightly larger for the impregnated samples. In all the three tests the polarisation resistance depends strongly on the atmosphere. Independent of whether the cells are impregnated or not the lowest polarisation resistance is at all temperatures found in 1000 ppm NO + 10% O_2. The highest polarisation resistance is below 400 °C found in 10% O_2, and above 400 °C in 1000 ppm NO. For the blank cell stack the polarisation resistance consistently decreased with increasing temperature, whereas for the KNO_3-impregnated samples an increase in the polarisation resistance was observed from 450 °C to 500 °C in 1000 ppm NO and 10% O_2, and for the MnO_x-impregnated cell an increase was observed from 400 to 450 °C in all atmospheres

Characteristics of processes/arcs

All the impedance spectra were fitted with 2-4 RQ subcircuits. In Figure 4 to Figure 6 representative examples from the fitting of the impedance spectra are shown, with the arcs used for the deconvolution of the spectra numbered according to the description in the results section. The shown spectra were recorded at 400 °C in

1000 ppm NO + 10% O_2 on cells from each of the three tests: 1) without impregnation; 2) with KNO_3 impregnation and 3) with MnO_x impregnation. In the following sections the results from fitting of the impedance spectra recorded during the three different tests will be described in more detail.

Blank cells:The impedance spectra recorded on the LSM15-CGO10 symmetric cells without impregnation were all fitted with 4 RQ-subcircuits at 300 °C, and 3 RQ-subcircuits at higher temperatures. Each RQ-subcircuit corresponds to an arc in the Nyquist plot, and in the following the arcs are numbered from 1 to 4, with number 1 being the arc observed at the highest frequencies (only observed at 300 °C), and number 4 being the arc observed at the lowest frequencies. A discussion of how the arcs may relate to different electrode processes will be found in the discussion section.

An overview of some of the characteristics of the arcs found during the fitting are stated in Table 3. In the first section of Table 3 the characteristic frequency of the individual arcs are stated at 300 °C and 500 °C together with the n-value of the constant phase element. With respect to the n-values it is noted the values were the same for arc 1, 2, and 4 independent of the atmosphere, whereas for arc 3 variation in the n-value was observed between the atmospheres. In the second section the activation energy for the process corresponding to each arc is stated together with the standard deviation and R^2-value of the linear regression, which was used for calculation of the activation energy. In this second section the stated activation energies are calculated from the results obtained in the entire temperature range from 300-500 °C, which means 5 points are used for the linear regression. Even though the R^2-values were close to 1 a small bend at 400 °C was observed on the Arrhenius plot for arc 3 in 1000 ppm NO and 1000 ppm NO + 10% O_2, se Figure 7 for an example. Since this small bend was consistently observed for all 4 cells, it could reflect a change in the process around 400 °C.

A comparison between the activation energies for arc 2 shows an activation energy of 0.78 eV in 1000 ppm NO, which is close to the activation energy observed in 1000 ppm NO + 10% O_2, but deviates from the 0.96 eV activation energy which is observed for process 2 in 10% O_2.

Finally, with respect to arc 4, no activation energy could be calculated in 1000 ppm NO, as no linear Arrhenius plot could be made from the fitting results. This was likely because this low frequency arc in 1000 ppm NO was distorted by a continued degradation. The activation energy for arc 4 was in 10% O_2 significantly higher when compared to 1000 ppm NO + 10% O_2, independent of whether the entire temperature range or only the higher part of the temperature range was considered.

KNO_3 impregnated cells: The impedance spectra recorded on the 3 symmetric LSM15-CGO10 cells impregnated with KNO_3 could all be fitted with between 2 and 4 RQ-subcircuits. Independent of the atmosphere, a small arc at very high frequencies was observed at 300 and 350 °C on all spectra. In 1000 ppm NO and in 10% O_2 two arcs/processes were consistently observed at all temperatures. These two arcs are named arc 3 and arc 4 in Table 4, but so far in the text it is not considered, whether these arcs represents the same processes or not in the different atmospheres. In addition to these two arcs in 1000 ppm NO, one additional smaller arc is observed at 350 °C (arc 2) and in the temperature range 400-500 °C a quite large arc (arc 5) appear at the lowest frequencies. Due to the limited temperature range at which arc 2 and arc 5 were observed it was not possible to calculate any activation energy for these two arcs.

In addition to the dominating arc 3 and 4 observed in 10% O_2, a smaller high frequency arc is observed at 500 °C, but also for this arc no activation energy can be calculated as the arc was only observed at one temperature.

In 1000 ppm NO + 10% O_2 3 arcs are consistently observed at all temperatures (arc 2, arc 3 and arc 4) and in addition to these arcs a small arc (arc 5) is observed in the temperature range 400-500 °C.

An overview of the arcs found in the different atmospheres, their characteristic frequencies, n-values and activation energies are found in Table 4. It should be noted only for arc 4 in 1000 ppm NO data recorded at 500 °C were used in the calculation of the activation energies, for all the other arcs the data at 500 °C was excluded from the calculation, as these data did not show linearity on the Arrhenious plot used for the calculation of the activation energy.

MnO_x-impregnated cells: Due to an insufficient number of datapoints and an apparent change in some of the processes at 400 °C, no activation energies could be calculated for the processes in 1000 ppm NO on the cells impregnated with MnO_x. In both 10% O_2 and 1000 ppm NO + 10% O_2 up to 4 arcs were identified in the impedance spectra. In both atmospheres a small arc, denoted arc 1, was observed at the high frequencies at 300 and 350 °C. Two arcs, denoted arc 3 and arc 4 were consistently observed at all temperatures and in addition to this an extra arc denoted arc 2 was on some of the spectra observed in the frequency region between arc 1 and arc 3. In 10% O_2 arc 2 was consistently observed in the temperature range 300-400 °C, which made it possible to calculate the activation energy for this arc. In 10% O_2 the Arrhenious plot for arc 3 showed an abrupt change between 400 and 450 °C, for this reason the activation energy could only be calculated based on the resistances in the region 300-400 °C.

Near-equivalent capacitance (C_ω)

From the fitting results the the near-equivalent capacitances C_ω were calculated for the individual arcs. In Table 6 to Table 8 the results for the different atmospheres are stated. It is observed there is no significant difference between the C_ω of the blank and the impregnated samples.

Only for the blank cells a consistent trend was observed with respect to the temperature dependency of the C_ω in the three atmospheres. In 1000 ppm NO the C_ω for both arc 2, arc 3 and arc 4 increased with temperature. In 10% O_2 the C_ω of arc 2 and arc 3 remained constant with temperature, whereas for arc 4 a slight decrease in C_ω was observed. In 1000 ppm NO + 10% O_2 the C_ω of arc 2 stayed more or less constant, whereas for both arc 3 and arc 4 an increase in the C_ω was observed with temperature.

Flow variations

At 500 °C flow variations were made in the three different atmospheres: 1000 ppm NO, 10% O_2 and 1000 ppm NO + 10% O_2 in all three tests. The flow variation was made by first recording an impedance spectrum in 100 ml/min gasflow, and immediately thereafter record an impedance spectra in 50 ml/min gasflow. In Table 9 the percentage change in resistance between the different flow rates is stated for the different arcs. A negative value corresponds to a smaller resistance in 50 ml/min and a positive value corresponds to a larger resistance in 50 ml/min compared to in 100 ml/min. In the NO-containing atmospheres the largest change in arc resistance is found for the arc observed at the lowest frequencies, and consistently the arc resistance decreases with decreasing flow rate. For the MnO_x-impregnated sample no measurements were made in 10% O_2, for this reason those results are missing in the Table 9.

Concentration change

During the test of the LSM15-CGO10 cells without impregnation, variations were made in the both the NO concentration and the O_2 concentration at 500 °C. At first the NO content was kept constant at 1000 ppm NO while the oxygen concentration was varied in the order 10, 5 and 15% O_2. Secondly the oxygen concentration was kept constant at 10% and the NO content was varied in the order 1000, 500 and 1500 ppm NO. The resistances and C_ω corresponding to the concentration variations are stated in

Table 10 for the variation in oxygen concentration and in Table 11 for the variation in NO concentration. With increasing oxygen content no influence is observed on the resistance of arc 2, a small decrease is observed in the resistance of arc 3, and a significant decrease in the resistance of arc 4 is observed. Only the C_ω of arc 4 appear to depend on the oxygen content, the C_ω of this arc appear to increase with increasing oxygen content. The resistances change with increasing NO concentration in a manner similar to when the oxygen content increases: the resistance of arc 2 remain unchanged, the resistance of arc 3 decreases slightly and the resistance of arc 4 decreases significantly. With respect to the C_ω and the influence of increasing NO concentration the C_ω of arc 2 remains constant but increases for arc 4, a behaviour similar to what was observed with increasing O_2 content. However for arc 3 the C_ω appears to decrease with increasing NO content, a behaviour which was not observed with an increase in the O_2 content.

Degradation

Degradation during the entire cell test was estimated from impedance spectra recorded in the beginning and the end of the cell test. The spectra were recorded at 300 °C in 1000 ppm NO and 10% O_2. In Table 12 the average serial and polarisation resistances obtained from the spectra are stated. In the blank test a minor increase is observed in both the serial resistance and the polarisation resistance during the cell test. For the cells impregnated with KNO_3 a minor decrease is observed in the serial resistance, and 51% increase is observed in the polarisation resistance. The cells impregnated with MnO_x show a significant degradation in the serial resistance, and a huge degradation (>3000%) in the polarisation resistance.

Since an increase was observed in the polarisation resistance for all the three tests, it was of interest to estimate which of the arcs/processes mainly contributed to this degradation. For this reason the change in the resistance of each arc was calculated and divided by the total change in the polarisation resistance. The result

from this calculation is shown in Figure 8, where positive values means the arc resistance increases and negative values the arc resistance decreases.

For the blank test the relatively small increase in polarisation resistance was equally caused by an increase in the resistance of arc 2 and 4. For the samples impregnated with KNO_3 the change in polarisation resistance was caused by an increase in the resistance of arc 4, and a decrease in the resistance of arc 3. In the test with MnO_x-impregnated samples only 3 arcs were observed at 300 °C, and the increase in polarisation resistance in this test was entirely caused by an increase in the resistance of the arc labelled 4. When comparing all three tests it is a consistent trend the increase in polarisation resistance either is solely or to a large extent explained by an increase in the resistance of arc 4.

Demounting

When the samples were demounted no visible change was seen before and after testing on the cells without impregnation and the cells impregnated with KNO_3. In contrast to this a very obvious change was observed between before and after cell testing on the cells impregnated with MnO_x. After the test these cells had become extremely brittle, and were all cracked into tiny pieces when they were demounted. It should be noted this only was seen for the three cells subjected to electrochemical cell testing, whereas the fourth cell, which only had experienced the temperature profile, at the demounting looked exactly as before testing.

SEM characterisation

SEM images were recorded on the cells before and after the electrochemical cell testing. In addition to this images were recorded on impregnated cells which had experienced the same temperature profile as the electrochemically tested cells, in order to investigate if changes observed in the microstructure mainly should

be ascribed to electrochemical cell testing or to the temperature profile experienced by the cells during the testing.

The blank sample before cell testing shows a fairly smooth surface on the electrode grains and the porosity evenly distributed in the electrode (Image A1). In the electrode impregnated with KNO_3 the KNO_3 is present in the electrode in big lumps with a slightly porous surface (Image B1). In the areas where the KNO_3 lumps are present, they more or less seem to block the electrode porosity, but most of the electrode is left without any sign of the KNO_3. After the electrochemical testing and also when the cell only had experienced the temperature profile as the tested cells, the areas with KNO_3 filling the porosity had disappeared, and the electrodes looks like the un-impregnated electrodes (Image B2 and Image B3). In the electrode impregnated with MnO_x the MnO_x appear to be present as fine nanoparticles distributed through the entire electrode before testing (Image C1). After the electrochemical cell testing a significant change is observed in the electrode microstructure, where bigger, round nanoparticles with a diameter around 50 nm are observed on the grain surfaces, which at the same time appear to have a rougher surface (Image C2). Yet another microstructure is found on the sample which only was subjected to the heat treatment. On this sample the nanoparticles seem to have vanished and the electrode appear similar to a blank, non-impregnated electrode (Image C3).

Discussion

Cylic voltammetry

One of the reasons why the cyclic voltammetry was made, was in order to see if oxidation and/or reduction of the KNO_3/K_2O NO_x storage compound could be observed on the CVs, as this has previously been observed on a similar system (37). In the cyclic voltammograms recorded in this work, a peak appeared only in NO containing

atmosphere at 400 and 450 °C on the KNO_3-impregnated samples. It seems likely this peak may be ascribed to the NO_x-storage compound. The fact this peak is only observed in 1000 ppm NO and not in 1000 ppm NO + 10% O_2, could be explained by presence of O_2 making it more favourable to reduce O_2 compared to reduce KNO_3.

When the current densities for the three tests obtained during cyclic voltammetry are compared to the polarisation resistances, the highest current densities are observed for the impregnated tests with also had the lowest polarisation resistances determined from the EIS. This indicates the information gained from the EIS recorded at OCV may also to some extent be applicable to the situation when the cells are under current load.

EIS results - Identification of processes

Blank cells: On the LSM15-CGO10 cells without impregnation 4 processes were identified to contribute to the polarisation resistance at 300 °C, and 3 processes to contribute at higher temperatures. In order to identify these processes comparison will be made to literature, and the effect of varying the atmosphere and the flow rates will be taken into consideration.

Starting from the high frequency end of the impedance spectra, arc 1 with a summit frequency around 20000 Hz is observed in all atmospheres, but only at 300 °C. The n-value of the arc is 0.9, and the near-equivalent capacitance is in the range $3*10^{-7}$-$6*10^{-7}$ F/cm^2. As the summit frequency and the C_ω of this arc is independent on the atmosphere, the arc is likely ascribed to transport of oxygen intermediates/oxygen ions between the electrolyte and the LSM and through the electrolyte part of the composite electrode, as identified by Jørgensen et al. (38) for LSM/YSZ electrodes and later also found for LSM/CGO electrodes (10).

In all atmospheres and temperatures an arc labelled arc 2 is identified. The n-value of the arc is in all atmospheres 0.45, but the C_ω of the arc shows must dependency on whether oxygen is present in the

atmosphere or not. While the C_ω in the oxygen containing atmospheres (10% O_2 and 1000 ppm NO + 10% O_2) remains more or less constant with increasing temperature, the C_ω in 1000 ppm NO continues to increase. The arc shows no dependency on the flowrate, or on variations in the pO_2 within the range 5-15% and variations in the NO conc. in the range 500-1500 ppm. In the temperature range 300-500 °C the calculated activation energy is close to 1 eV in 10% O_2, but only around 0.76 eV in the NO containing atmospheres. The difference in activation energy for arc 2 between the NO containing atmospheres and 10% O_2 could indicate the arc represents one process in NO containing atmospheres and another process in 10% O_2. In 10% O_2 the activation energy around 1 eV corresponds well with the activation observed by Jørgensen et al. for the transport/transfer of oxygen intermediates between the LSM and the electrolyte material and through the electrolyte material. As explained by Jørgensen et al. (38) these processes may give rise to two arcs in the impedance spectrum, named arc A and arc B, and could for this reason account for both arc 1 and arc 2 observed in 10% O_2 in this work. However, on the impregnated samples arc 2 decreases significantly or disappears entirely (described later in the article), which would not be the case if arc 2 was related to oxygen ion transport in the CGO. For this reason arc 2 is so far ascribed to one of the processes dissociative adsorption, diffusion or charge transfer at the TPB.

Arc 3 was fitted with the n-values 0.68 (1000 ppm NO), 0.54 (10% O_2) and 0.69 (1000 ppm NO +10% O_2). The C_ω in 1000 ppm NO for arc 3 behaved similar to for arc 2, with a continued increase with temperature. In 10% O_2 and 1000 ppm NO + 10% O_2 some divergence is found in the C_ω below 400 °C, with the lowest C_ω found in 1000 ppm NO + 10% O_2, but at 400 °C and above the C_ω in these two atmospheres become almost equal. If only the temperature range 400-500 °C is considered the activation energy of this arc is close to 1 eV in all 3 atmospheres, but if the lower temperatures are included in the calculation of the C_ω, the activation energies in the NO containing atmospheres decreases to 0.69. The decrease in the calculated activation energy is likely due a shift in the process around 400 °C, visible as a bend on the Arrhenious plot for the NO-containing

atmospheres. Arc 3 shows no dependency on flow variations, but the resistance decreases slightly when the oxygen content is increased from 5-15% or the NO content is increased from 500 to 1500 ppm NO. The change between 5 to 15% oxygen does not affect the C_{ω}, whereas the increase in NO content from 500 to 1500 ppm decreases the C_{ω} of arc 3 slightly. Arc 3 appears to be dependent on the atmosphere and show no dependency on the flow rate. In the literature a process being dependent on the atmospheres is dissociative adsorption, transfer of species at the triple-phase- boundary (TPB) and surface diffusion (38). The activation energy for this process in air was by Jørgensen et al. reported to be in the range 1.5-2 eV (38), which is above the reported activation energy of 1 eV in 10% O_2 reported in this work. But Werchmeister et al. reported the activation energy for the TPB process to be 0.64 eV in 1% NO, (10), which shows the activation energy of this process is lower in NO compared to in air. As mentioned, a bend was observed on the Arrhenious curve in NO containing atmospheres around 400 °C. Combined with the attribution of arc 3 to TPB-related proceeses, a possible explanation of the bend could be a change in the adsorbed NO_x-species with increasing temperature. In-situ DRIFT measurements of NO adsorption on a model NO_x-storage catalyst and on La_2O_3 showed a change in the adsorbed NO_x-species during temperature increase from 300 °C to 500 °C (39, 40). This makes it likely a similar change will be observed when NO_x is adsorbed on LSM15-CGO10 electrodes, and a change in the adsorbed NO_x species would likely affect processes related to the TPB process like surface diffusion and dissociative adsorption, thereby causing the observed bend on the Arrhenious curved for arc 3.

The arc observed at the lowest frequencies, arc 4, behaves quite differently depending on the atmosphere, but is in all cases fitted with the n-value 0.89. In the NO containing atmospheres the arc resistance decreases with decreasing flowrate, most significantly when only 1000 ppm NO is present. No activation energy could be calculated for this arc in 1000 ppm NO, but the fact the arc decreases with decreasing flow rate makes it likely the arc is a NO_2 conversion arc as previously reported by Werchmeister et al. (10). The NO_2 conversion arc was

reported to have an activation energy of 0.34 eV in 1% NO in Ar (10). This is below the activation energy 0.88 eV reported for arc 4 in 1000 ppm NO + 10% O_2 in this work.

KNO_3-impregnated cells: The impedance spectra recorded on the KNO_3-impregnated cell were fitted with between 2 and 4 RQ-subcircuits. Compared to the spectra recorded on the blank cells, the impedance spectra recorded on the KNO_3-impregnated cells have an additional smaller arc present in the low frequency region in 1000 ppm NO + 10% O_2.

In the following the processes will be described one by one, starting from high frequency and with the arcs numbered from 1 to 5 as in the results section.

Independent of the atmosphere, a high frequency arc is observed at 300 and 350 °C, with a summit frequency around 20000 Hz at 300 °C. The n-value of the arc is 0.8, the C_ω around $1.2x10^{-7}$ F/cm^2 at 300 °C, and since the summit frequency and C_ω does not depend on the atmosphere, the arc is likely ascribed to transport of oxygen intermediates/oxygen ions between the electrolyte and the LSM and through the electrolyte part of the composite electrode (38).

In 1000 ppm NO + 10% O_2 an arc labelled arc 2 is consistently observed at all temperatures. The arc is fitted with the n-value 0.6. The arc does not change when the flow is changed at 500 °C, and the activation energy of the process corresponding to the arc is close to 1 eV. This activation energy is lower than the activation energy for the TPB-process of 1.5-2 eV reported by Jørgensen et al. (38) for LSM/YSZ composite electrodes in air, and higher than the activation energy of 0.64 eV reported by Werchmeister et al. (10) for the TPB-process in 1% NO on LSM15/CGO10 composite electrodes. It should be noted in the two other atmospheres, 1000 ppm NO and 10% O_2, an arc labelled arc 2 is also found in some of the impedance spectra, but since this arc is so rarely observed no activation energy could be calculated, and it will not be discussed further.

Arc 3 is consistently observed at all temperatures in all atmospheres. In 1000 ppm NO and 10% O_2 the arc is fitted with n-value 0.59, whereas in 1000 ppm NO + 10% O_2 the n-value 0.7 is used. The C_ω is in all atmospheres in the range $1x10^{-5}$-$8x10^{-4}$ F/cm^2. In 1000 ppm NO and 10% O_2 the activation energy of the arc is 1.16 eV, whereas in 1000 ppm NO + 10% O_2 the activation energy is only 0.76 eV. As described for arc 2, these activation energies lies between the activation energies reported for the TPB process by Jørgensen et al. (38) and Werchmeister et al. (10) .

In addition to arc 3 arc 4 is the only other arc consistently observed in all atmospheres at all temperatures. In the three different atmospheres the arc is fitted with the n-values 0.76 (1000 ppm NO), 0.85 (10% O_2) and 0.90 (1000 ppm NO + 10% O_2). The C_ω of the arc is in the range $4x10^{-4}$-$4x10^{-2}$ F/cm^2. The activation energies found for the arc were 0.42 eV (1000 ppm NO), 1.4 eV (10% O_2) and 0.52 eV (1000 ppm NO + 10% O_2). When the flow rate is decreased, the arc resistance decreases in the NO containing atmospheres, but stays more or less constant in 10% O_2. The significant difference in activation energy observed between the NO-containing atmospheres and in 10% O_2 combined with the different behaviour during the flow rate variations, indicates this arc represents a different process depending on whether NO is present is not. Exactly which process the arc represents is hard to decide, as the activation energies for the arc lies in between the activation energies determined by Werchmeister et al. for the arc related to the TPB-processes (0.64 eV) and the NO_2 conversion arc (0.34 eV) in 1% NO (10). It can also be discussed whether the decrease in arc resistance with decreasing flowrate is big enough to be considered a true change, or may just be a false effect caused by a change in resistance of the low frequency arc 5 located next to arc 4.

Arc 5 appear in the low frequency region in the temperature range 400-500 °C in 1000 ppm NO and 1000 ppm NO + 10% O_2. Whereas arc 5 in 1000 ppm NO + 10% O_2 is a small arc adjacent to the much bigger arc 4, the result is quite different in 1000 ppm NO, where arc 5 is the major contributor to the cell resistance. The arc was

fitted with the n-value 0.88 in 1000 ppm NO and 0.97 in 1000 ppm NO + 10% O_2. The C_ω of the arc decreased strongly with temperature in both atmospheres, in 1000 ppm NO from around 1 to $4x10^{-3}$ F/cm^2, and in 1000 ppm NO + 10% O_2 from 1 to around $7x10^{-2}$ F/cm^2. Of all the arcs identified on the KNO_3 impregnated sample arc 5 shows the most significant dependency on flow rate, with a decrease in flow rate causing a decrease in arc resistance. The dependency on flow rate combined with a high n-value could indicate the arc is an NO_2 conversion arc as previously reported by Werchmeister et al. (10), on the other hand the arc could also be due to a process related only to the presence of impregnated KNO_3 and NO in the atmosphere, this will be discussed further in the section "Effect of impregnation – overall comparison of tests"

MnO_x-impregnated cells:The spectra recorded on the MnO_x-impregnated cells are all fitted with 2-4 RQ-subcircuits. As previously written, no activation energies could be calculated for the processes in 1000 ppm NO, for this reason only the results found in 10% O_2 and 1000 ppm NO + 10% O_2 will be discussed.

Consistent with the results from the blank and the KNO_3-impregnated cells, a high frequency arc, labelled arc 1, is observed at 300 °C and 350 °C on the MnO_x-impregnated cells. The summit frequency of this arc is in the range 30000-50000 Hz, which is higher than the summit frequency around 20000 Hz observed for this arc in the other tests. Again the arc will be ascribed to transport of oxygen intermediates/oxygen ions between the electrolyte and the LSM and through the electrolyte part of the composite electrode (38), as the presence only at lower temperatures and the distinct separation to the rest of the impedance spectra seems to be quite characteristic features of this arc.

On the impedance spectra recorded in 10% O_2 an arc labelled arc 2 is observed in the temperature range 300-400 °C. The arc is fitted with the n-value 0.65 and the activation energy is calculated to be 0.87 eV. In 1000 ppm NO + 10% O_2 an arc labelled arc 2 is only observed a few times, and the arc will for this reason not be discussed any further for this atmosphere.

The arc labelled arc 3 is consistently observed at all temperatures in both 10% O_2 and 1000 ppm NO + 10% O_2. In 10% O_2 the arc is fitted with n-value 0.59, and the activation energy is calculated to 1.18 eV, while in 1000 ppm NO + 10% O_2 the arc is fitted with n-value 0.61 and the activation energy is calculated to 0.78 eV. In both atmospheres the C_ω of the arc is found in the range $1x10^{-5}$-$1x10^{-3}$ F/cm^2. The difference in activation energy between arc 3 in the two atmospheres indicates the arc represents two different processes, but when compared to Jørgensen et al. (38) and Werchmeister et al. (10) it seems likely the process in both atmospheres is related to dissociative adsorption, transfer of species at TPB and surface diffusion. The difference between the two atmospheres is then likely the species which participate in the reactions at the TPB, and it seems plausible NO_x-species participate in these reactions when NO is present in the atmospheres.

Finally arc 4 is observed at all temperatures in both atmospheres as well. In 10% O_2 the arc is characterised by n-value 0.73, activation energy 0.64 eV and C_ω in the range $8x10^{-5}$-$1x10^{-3}$ F/cm^2. In 1000 ppm NO +10% O_2 the arc is characterized by n-value 0.74, activation energy 0.38 eV and C_ω in the range $1x10^{-5}$-$8x10^{-4}$ F/cm^2. During the flow variation the arc resistance decrease with decreasing flow rate in 1000 ppm NO +10% O_2, which together with the low activation energy is in agreement with characteristics Werchmeister et al. found for the NO_2 conversion arc (10). Contrary to the observations made by Werchmeister al. (10), who as expected for a conversion arc observed an n-value close to 1, the NO_2-conversion arc observed on the MnO_x-impregnated samples is lower, around 0.74.

Effect of impregnation – overall comparison of tests

As stated in the beginning of the results section, impregnation with KNO_3 and MnO_x significantly decreased the polarisation resistance of LSM15/CGO10 electrodes in the temperature range 300-450 °C, both in 1000 ppm NO, in 10% O_2 and in 1000 ppm NO + 10% O_2. It would be of great interest to understand, which of the electrode processes are affected by the impregnation and especially how they are affected. For the NO-

containing atmospheres it also of interest to see, if any NO-storage effect can be found for the KNO_3 and/or MnO_x-impregnation. For this reason the preceding description of fitting of impedance spectra was given, as these results may yield information on the effect of the impregnation on the electrode processes. In the following the impedance results from the three tests will be compared, and the effect of the impregnations on the individual processes will be discussed. An underlying assumption in the discussion is the majority of the processes identified in the three tests will be the same, as the impregnations are expected to affect the electrode processes but not totally alter all of them.

To summarize the results, all the impedance spectra were fitted with 2-4 RQ-subcircuits, independent of whether the samples were impregnated or not. Independent of the atmosphere, a high frequency arc (Arc 1) was observed on all spectra at low temperatures, and ascribed to transport/transfer of oxygen intermediates/oxide ions between the LSM and CGO and through the CGO electrolyte. In both the NO containing atmospheres a NO_2 conversion arc (arc 4) was found in the low frequency end of the impedance spectra in all tests. In between the just-described high frequency arc and low frequency arc, two other arcs (arc 2 and arc 3) were present in 1000 ppm NO and in 1000 ppm NO + 10% O_2. Both arcs are ascribed to processes at or nearby the TPB (adsorption/diffusion/charge transfer). In addition to these arcs one more arc is observed in NO-containing atmospheres on the KNO_3 impregnated sample. As this arc is only observed on the KNO_3-impregnated sample, and only when NO is present in the atmosphere, it seems reasonable to ascribe the arc to a NO_x-storage process, or at least a process related to interaction between the NO and the impregnated KNO_3. It should be pointed out, the resistance of both arc 4 and arc 5 decreased with decreasing flow rate in NO containing atmospheres. For arc 4 this was explained in accordance with the results from Werchmeister et al who ascribed the arc to conversion of the intermediate NO_2 formed catalytically from the NO on the LSM (10). For arc 5, which in this work is ascribed to a NO_x-storage process, a similar dependence on the flow rate, i.e. the concentration of NO_2, could be expected for the following reason: In conventional NSR-catalysis the

reaction sequence is reported to consist first of catalytic conversion of NO to NO_2 on the platinum sites, and subsequent storage of the NO_2 on the NO_x-storage compound (41, 42). On LSM-electrodes combined with a NO_x-storage compound a similar mechanism would be catalytic conversion of NO to NO_2 on LSM instead of platinum, and subsequent storage/adsorption of the NO_2 on the NO_x-storage compound. A decrease in flow rate would in this case decrease the resistance of the NO_x-storage process due to the higher concentration of NO_2, as observed in this work.

In the atmosphere with 10% O_2 two to three arcs are observed in addition to the high frequency arc. From the results obtained in this work it is not possible with certainty to assign these arcs to specific electrode processes, but they are so far ascribed to processes at or around the TPB. It should be noted in literature it is reported gas phase diffusion resistance may be significant below 10% O_2 (43), i.e. at a pO_2 range close to the pO_2 during testing in this work. But as gas phase diffusion resistance is expected to be temperature independent (38), and all the processes identified in 10% O_2 show a strong temperature dependency, gas phase diffusion cannot explain any of the arcs observed in 10% O_2 in this work.

In order to evaluate if all the processes have been affected equally by the impregnation, it is useful to compare how the impregnation affects the resistance of the different arcs. In Figure 10 to Figure 12 the resistances found in 1000 ppm NO + 10% O_2 are shown for the three different tests, and it is observed how the impregnation causes a general decrease in resistance, with arc 4/the NO_2 conversion at 400 to 500 °C as the one exception.

Activation energies in 1000 ppm NO + 10% O_2

In addition to the change in resistances due to the impregnation the change in activation energies should also be considered. A change in the activation energy would usually be interpreted as a change in the reaction

mechanism, which for instance could be due to a different reaction intermediates, other available reactions sites etc. However a change in activation energy could also be the result from a change in the microstructure during the test. If the microstructure is dominated by impregnated nano-particles at low temperatures, and the microstructure becomes coarser at high temperatures, an apparent change in activation energy will be observed for processes dependent on the electrode microstructure. This change will be due to the micro structural changes and the correlated change in resistances, and not due to a change in the actual reaction mechanism.

In 1000 ppm NO +10% O_2 the activation energy of arc 2 has increased from 0.74 eV to 1.05 eV when the electrodes were impregnated with KNO_3. When the impregnation was made with MnO_x, no activation energy could be calculated for arc 2, as the arc was only found on very few EIS spectra. This could indicate the MnO_x-impregnation decreased the resistance of arc 2 so much; the arc no longer can be separated on the impedance plot and no activation energy could be calculated.

In the same atmosphere, none of the impregnations seemed to alter the activation energy of arc 3, as it only varies between 0.69 (blank), 0.76 (KNO_3 imp.) and 0.78 (MnO_x imp.) which will be considered within the uncertainty of the experiment and the fitting. Arc 3, which was ascribed to a TPB related process, has for this reason not changed reaction mechanism (E_a is constant) due to the impregnation, but the resistances of the arc has in general decreased, which would agree with the impregnations causing an increase in the triple-phase boundary length.

For arc 4/the NO_2 conversion arc no activation energy could be calculated for the KNO_3 impregnated sample, whereas for the MnO_x-impregnated sample the activation energy had decreased significantly, from 0.88 eV (blank sample) to 0.38 (MnO_x-impregnated sample). The decrease in activation energy for the MnO_x-

impregnated sample could be explained by the MnO_x increasing the catalytic conversion of NO to NO_2 thereby increasing the NO_2 concentration in the electrode.

Activation energies in 10% O_2

Looking at the effect of the impregnation on the processes in 10% O_2 both impregnations seemed to decrease the activation energy of arc 3, whereas for arc 4 the KNO_3 impregnation left the activation energy unchanged while the MnO_x impregnation decreased the activation energy of the arc. So far both arc 3 and arc 4 are ascribed to processes related to the TPB. For the arc 3 process both impregnations seem to introduce or enhance a reaction path way with lower activation energy, whereas for arc 4 this only seem to be the case for the MnO_x impregnation.

Finally, with respect to the effect of impregnating with MnO_x and KNO_3, it was unexpected the impregnation with KNO_3 had such a significant impact on the resistances not only in the NO containing atmospheres, but also in 10% O_2. This was unexpected as KNO_3 was expected to interact with NO during the NO_x-storage, but not to have any effect on electrode reactions involving only oxygen species. Also the fact the MnO_x and KNO_3 impregnation was distributed so differently in the electrodes before testing made it quite surprising both impregnations in general decreased the resistances contributing to the polarisation resistances. This shows, a clear understanding of how impregnation in general and especially the KNO_3 impregnation affects the electrode processes is still missing. To clarify this more experiments are needed, as a first suggestion the impregnation of KNO_3 should be improved to get the KNO_3 more evenly distributed in the electrode, and more impedance spectra should be recorded with variations in the NO and O_2 concentration to gain more insight into the processes occurring in the KNO_3 impregnated electrodes.

Degradation

As shown in the results section the degradation of the impregnated samples is in general larger compared to the blank samples.. The majority of the degradation in the polarisation resistance was caused by an increase in the resistance of arc 4, which is ascribed to the NO_2 conversion process. This resistance increase could be explained in two different ways:

1. The LSM had lost ability to convert NO to NO_2 during degradation, thereby decreasing the NO_2 concentration.
2. The ability of the electrodes to convert NO_2 had decreased during testing.

Of course a combination of the two cases above could be a possibility as well.

For the KNO_3-impregnated sample a 51% increase in the polarization resistance was observed. This increase was due to a combination of a resistance decrease for process 3 (related to TPB-processes) and a resistance increase for arc 4 (the NO_2 conversion arc). From the SEM images it is clear a significant redistribution of the impregnated KNO_3 has taken place, which may correlate with the decrease of the TPB resistance. The increase in the arc 4 resistance may be explained by point 1 or point 2 stated above.

The SEM images reveal a clear change in the microstructure, when the images recorded on the MnO_x-impregnated sample before and after testing are compared. The microstructural change, deterioration of the electrode grain surfaces and formation of round shaped particles, is obviously related to the polarisation of the electrode, as the same change in microstructure is not observed for cells which had only been heat treated as the tested samples. Lee et al. showed manganese ions in LSM lattice and interstitial sites were reduced to Mn^{2+} under cathodic polarisation, which led to the formation of oxygen ion vacancies on the LSM electrode surface (44). This, combined with high surface mobility of Mn^{2+} ions, was by Jiang et al. used to explain the formation of sphere-like structures on LSM cathodes which had been polarised at 500 mA at 1000 °C in 3 hours (45). A similar phenomenon could explain the changes in microstructure observed in this work: During the

polarisation, the manganese ions in the impregnated MnO_x may be reduced to Mn^{2+}. If a large excess of manganese ions are present at the LSM surface, and they all are reduce to Mn^{2+}, a large number of oxygen vacancies will be created in the LSM lattice. The diffusion of manganese ions and oxygen vacancies may lead to formation of sphere shaped particles and weakening of the bonding between the particles in the electrode similar to the observations made by Jiang et al. (45). This could then explain both the change in microstructure observed on the SEM images and the reduced mechanical strength of the MnO_x-impregnated cell after the electrochemical characterisation. On the MnO_x-impregnated cells only subjected to the heat-treatment and not to the electrochemical testing, no trace of the impregnated MnO_x was observed in the electrode, which looked like the electrode of the un-impregnated cell. This may be due to incorporation of the impregnated MnO_x-into the LSM of the electrode during the heat treatment.

Conclusion

Both EIS and cyclic voltammograms show impregnation with KNO_3 introduce a NO_x-storage process in the electrode; this storage process apparently takes places after NO_2 has been formed catalytically on the electrode. Impregnation with MnO_x does not introduce a NO_x- storage process, but both the MnO_x- and the KNO_3-impregnation cause a significant decrease in the polarization resistance of the electrodes in both 1000 ppm NO, 10% O_2 and 1000 ppm NO + 10% O_2. The decrease in polarization resistance is caused both by a decrease in resistance of the processes related to the TPB, and a decrease in the resistance of the NO_2 conversion process in the NO containing atmospheres. It is remarkable a general decrease in these resistances

is observed with both impregnations, even though the mictrostructure of the two impregnations appear fairly different. The impregnated samples degrade significantly more than the non-impregnated samples during testing. Based on SEM images and literature it is concluded the increased degradation follows from redistribution of the impregnated compound during testing, and with respect to the MnO_x-impregnated sample formation and diffusion of Mn^{2+} and oxygen vacancies may explain the severe degradation observed.

Acknowledgements

This work was supported by the Danish Strategic Research Council under contract no. 09-065186. Technicians at the Fuel Cell and Solid State Chemistry Division, Technical University of Denmark, are thanked for invaluable help and advice.

References

1. Ecopoint Inc., *http://www.dieselnet.com/standards/eu/hd.php, 2011 6/21* (2009).

2. K. Wark, C. F. Warner and W. T. Davis, *Air Pollution Its Origin and Control, Third edition*, p. 573, Addison Wesley Longman, Inc., USA (1998).

3. K. Skalska, J. S. Miller and S. Ledakowicz, *Sci.Total Environ.,* **408**, 19 (2010).

4. S. Pancharatnam, R. A. Huggins and D. M. Mason, *J.Electrochem.Soc.,* **122**, 7 (1975).

5. S. Bredikhin, K. Matsuda, K. Maeda and M. Awano, *Solid State Ionics.,* **149**, 3-4 (2002).

6. K. Hamamoto, Y. Fujishiro and M. Awano, *J.Electrochem.Soc.,* **155**, 8 (2008).

7. K. K. Hansen, H. Christensen and E. M. Skou, *Ionics.,* **6** (2000).

8. K. J. Walsh and P. S. Fedkiw, *Solid State Ionics.,* **93**, 1-2 (1996).

9. K. J. Walsh and P. S. Fedkiw, *Solid State Ionics.,* **104**, 1-2 (1997).

10. R. M. L. Werchmeister, K. K. Hansen and M. Mogensen, *J.Electrochem.Soc.,* **157**, 5 (2010).

11. K. K. Hansen, *Applied Catalysis B: Environmental.,* **100**, 3-4 (2010).

12. N. Takahashi, K. Yamazaki, H. Sobukawa and H. Shinjoh, *Applied Catalysis B-Environmental.,* **70**, 1-4 (2007).

13. T. J. Toops, D. B. Smith, W. S. Epling, J. E. Parks and W. P. Partridge, *Applied Catalysis B: Environmental.,* **58**, 3-4 (2005).

14. T. Lesage, J. Saussey, S. Malo, M. Hervieu, C. Hedouin, G. Blanchard and M. Daturi, *Applied Catalysis B: Environmental.,* **72**, 1-2 (2007).

15. V. G. Milt, M. L. Pissarello, E. E. Miró and C. A. Querini, *Applied Catalysis B: Environmental.,* **41**, 4 (2003).

16. R. Fricke, E. Schreier, R. Eckelt, M. Richter and A. Trunschke, *Topics in Catalysis.,* **30-1**, 1-4 (2004).

17. C. Lu, T. Z. Sholklapper, C. P. Jacobson, S. J. Visco and L. C. De Jonghe, *J.Electrochem.Soc.,* **153**, 6 (2006).

18. S. P. Jiang, Y. Y. Duan and J. G. Love, *J.Electrochem.Soc.,* **149**, 9 (2002).

19. K. K. Hansen, M. Wandel, Y. -. Liu and M. Mogensen, *Electrochim.Acta.,* **55**, 15 (2010).

20. J. M. Thomas and W. J. Thomas, *Principles and Practice of Heterogenous Catalysis*, p. 669, VCH Verlagsgesellschaft mbH, Weinheim, (1997).

21. A. J. McEvoy, *Solid State Ionics.,* **135**, 1-4 (2000).

22. C. W. Sun, R. Hui and J. Roller, *Journal of Solid State Electrochemistry.,* **14**, 7 (2010).

23. G. J. Janz, U. Krebs, H. H. Siegenthaler and R. P. T. Tomkins, *J. Phys. Chem. Ref. Data.,* **1**, 3 (1972).

24. O. Ghodbane, J. Pascal and F. Favier, *ACS Appl.Mater.Interfaces.,* **1**, 5 (2009).

25. M. Kertesz, I. Riess, D. S. Tannhauser, R. Langpape and F. J. Rohr, *Journal of Solid State Chemistry.,* **42**, 2 (1982).

26. J. H. Kuo, H. U. Anderson and D. M. Sparlin, *Journal of Solid State Chemistry.,* **87**, 1 (1990).

27. S. R. Wang, T. Kobayashi, M. Dokiya and T. Hashimoto, *J.Electrochem.Soc.,* **147**, 10 (2000).

28. L. A. Chick, L. R. Pederson, G. D. Maupin, J. L. Bates, L. E. Thomas and G. J. Exarhos, *Mater Lett.,* **10**, 1-2 (1990).

29. M. Maneva and N. Petroff, *J Therm Anal.,* **36**, 7-8 (1990).

30. W. M. Haynes and D. R. Lide, *CRC Handbook of Chemistry and Physics, 91st edition*, Tayler and Francis Group, LCL (2010-2011).

31. J. Kaspar, P. Fornasiero and N. Hickey, *Catalysis Today.,* **77**, 4 (2003).

32. B. A. A. L. van Setten, M. Makkee and J. A. Moulijn, *Catalysis Reviews: Science and Engineering.,* **43**, 4 (2001).

33. D. Johnson and Scribner Associates, **ZView2, 3.1 c** (1990-2007).

34. E. Barsoukov and J. R. Macdonald, *Impedance Spectroscopy Theory, Experiment and Applications, second edition*, John Wiley and Sons, Inc., Hoboken, New Jersey (2005).

35. T. Jacobsen, B. ZachauChristiansen, L. Bay and S. Skaarup, *High Temperature Electrochemistry: Ceramics and Metals.,* (1996).

36. S. Omar, E. D. Wachsman, J. L. Jones and J. C. Nino, *J Am Ceram Soc.,* **92**, 11 (2009).

37. A. de Lucas-Consuegra, A. Caravaca, P. Sanchez, F. Dorado and J. L. Valverde, *Journal of Catalysis.,* **259**, 1 (2008).

38. M. J. Jørgensen and M. Mogensen, *J.Electrochem.Soc.,* **148**, 5 (2001).

39. Y. Ji, T. J. Toops, J. A. Pihl and M. Crocker, *Applied Catalysis B: Environmental.,* **91**, 1-2 (2009).

40. B. Klingenberg and M. A. Vannice, *Applied Catalysis B-Environmental.,* **21**, 1 (1999).

41. N. Takahashi, H. Shinjoh, T. Iijima, T. Suzuki, K. Yamazaki, K. Yokota, H. Suzuki, N. Miyoshi, S. Matsumoto, T. Tanizawa, T. Tanaka, S. Tateishi and K. Kasahara, *Catalysis Today.,* **27**, 1-2 (1996).

42. W. S. Epling, L. E. Campbell, A. Yezerets, N. W. Currier and J. E. Parks, *Catalysis Reviews-Science and Engineering.,* **46**, 2 (2004).

43. S. B. Adler, J. A. Lane and B. C. H. Steele, *J.Electrochem.Soc.,* **143**, 11 (1996).

44. H. Y. Lee, W. S. Cho, S. M. Oh, H. D. Wiemhofer and W. Gopel, *J.Electrochem.Soc.,* **142**, 8 (1995).

45. S. P. Jiang and J. G. Love, *Solid State Ionics.,* **158**, 1-2 (2003).

Table 1. Current densities in mA/cm^2 observed at the cyclic voltammograms (2. scan) at 0.9 V polarisation in 1000 ppm NO +10% O_2 on blank, KNO_3 and MnO_x impregnated LSM15-CGO10 symmetric cells. The numbers stated in the parenthesis are the uncertainties.

Temp. [°C]	Blank	KNO3	MnO_x	
			Cell A and C	Cell D
300	0.46(0.04)	0.6 (0.03)	3.03(0.06)	2.8(0.1)
350	1.2(0.1)	3(0.1)	7(1)	7.6(0.4)
400	4.2(0.3)	9(0.4)	12(3)	15.2(0.8)
450	10.3(0.5)	18(3)	12(3)	25(1)
500	27(1)	30(1)	13(3)	63(5)

Table 2. Average polarisation resistances in 1000 ppm NO, 10% O_2 and 1000 ppm NO + 10% O_2 obtained for symmetric LSM15-CGO10 cells without impregnation (labelled "blank") with KNO_3 impregnation and with MnO_x-impregnation. The values are stated in Ωcm^2.

	1000 pppm NO			10% O2			1000 ppm NO + 10% O2		
Temp. [°C]	Blank	KNO_3	MnO_x	Blank	KNO_3	MnO_x	Blank	KNO_3	MnO_x
300	$1.0 \cdot 10^4$	$4.1 \cdot 10^3$	$1.1 \cdot 10^3$	$1.8 \cdot 10^5$	$7.8 \cdot 10^4$	$4.2 \cdot 10^3$	$7.6 \cdot 10^3$	$3.2 \cdot 10^3$	$7.6 \cdot 10^2$
350	$4.2 \cdot 10^3$	$1.4 \cdot 10^3$	$4.5 \cdot 10^2$	$3.1 \cdot 10^4$	$5.1 \cdot 10^3$	$1.2 \cdot 10^3$	$2.2 \cdot 10^3$	$9.9 \cdot 10^2$	$3.5 \cdot 10^2$
400	$2.9 \cdot 10^3$	$9.7 \cdot 10^2$	$2.4 \cdot 10^2$	$5.8 \cdot 10^3$	$1.1 \cdot 10^3$	$4.3 \cdot 10^2$	$7.8 \cdot 10^2$	$5.1 \cdot 10^2$	$2.2 \cdot 10^2$
450	$2.0 \cdot 10^3$	$6.0 \cdot 10^2$	$1.1 \cdot 10^3$	$1.2 \cdot 10^3$	$2.1 \cdot 10^2$	$4.6 \cdot 10^2$	$3.1 \cdot 10^2$	$2.7 \cdot 10^2$	$2.3 \cdot 10^2$
500	$1.3 \cdot 10^3$	$9.4 \cdot 10^2$	$9.0 \cdot 10^2$	$2.6 \cdot 10^2$	$2.6 \cdot 10^2$	$3.2 \cdot 10^2$	$1.2 \cdot 10^2$	$1.4 \cdot 10^2$	$1.8 \cdot 10^2$

Table 3. Characteristics of the four arcs/RQ-subcircuits used during fitting of the impedance spectra recorded on symmetric LSM15-CGO10 cells. In the table n-value is the n-value of the CPE, Ea the activation energy, R^2 is the estimate of the linearity between the points used for the calculation of Ea, and the last column named

				Results at 300-500 °C		
Arc	Freq. at 300 °C	Freq. at 500 °C	n-value	Ea	Stdev	R^2
	Hz	Hz		eV		
1	19952		0.90			
2	9	137	0.45	0.78	0.02	0.997
3	3	4	0.68	0.69	0.07	0.962
4	0.3	0.08	0.89	?	?	?
1	18458		0.90			
2	7	1049	0.45	0.96	0.05	0.991
3	0.09	20	0.54	0.98	0.05	0.999
4	0.0007	0.8	0.89	1.29	0.05	0.992
1	21745		0.90			
2	22	492	0.45	0.74	0.02	0.993
3	5	27	0.69	0.69	0.01	0.972
4	0.8	2	0.89	0.88	0.02	0.984

Table 4. Characteristics of the arcs/RQ-subcircuits used during fitting of the impedance spectra recorded on symmetric LSM15-CGO10 cells impregnated with KNO_3. In the table n-value is the n-value of the CPE, Ea the activation energy and R^2 is the estimate of the linearity between the points used for the calculation of Ea.

					Results at 300-450 °C		
Atmosphere	Arc	Freq. at 300 °C Hz	Freq. at 500 °C Hz	n-value	Ea eV	Stdev	R
1000 ppm NO	1	19878		0.82			
	2			0.83			
	3	0.5	599	0.59	1.16	0.12	0.977
Also at 500 °C	4	0.05	8	0.76	0.42	0.14	0.984
	5		0.10	0.88	?	?	?
10% O2	1	21333		0.79			
	2			0.51			
	3	0.1	33	0.59	1.16	0.04	0.997
	4	0.002	1	0.85	1.40	0.18	0.983
1000 ppm NO + 10% O2	1	17370		0.81			
	2	47	7670	0.60	1.05	0.07	0.988
	3	2	48	0.70	0.76	0.08	0.974
	4	0.3	3	0.90	0.52	0.04	0.980
	5		0.3	0.97	?	?	?

Table 5. Characteristics of the arcs/RQ-subcircuits used during fitting of the impedance spectra recorded on symmetric LSM15-CGO10 cells impregnated with MnO_x. In the table n-value is the n-value of the CPE, Ea the activation energy and R^2 is the estimate of the linearity between the points used for the calculation of Ea. Due to an insufficient number of datapoints and an apparent change in the process no activation energies could be calculated for the 1000 ppm NO atmosphere, for which reason no results from this atmosphere is included in the table.

Atmosphere	Arc	Freq. at 300 °C Hz	Freq. at 500 °C Hz	n-value	Ea eV	Stdev	R	T. range
10% O2	1	36919		0.90				
	2	64		0.65	0.87	0.05	1.000	300-400 °C
	3	3.1	80	0.59	1.18	0.36	0.995	300-400 °C
	4	0.137	3	0.73	0.64	0.01	0.977	300-500 °C
1000 ppm NO + 10% O2	1	41585		0.87				
	2			0.50				
	3	42	129	0.61	0.78	0.02	1.000	300-500 °C
	4	3.8	6	0.74	0.38	0.05	0.967	300-500 °C

Table 6. C_ω in 1000 ppm NO in the temperature range 300 °C – 500 °C (for Arc 1 only for 300 °C). The values are stated in F/cm^2.

	Blank	KNO_3 imp.	MnO_x imp.
Arc 1	$2\cdot10^{-7}$-$3\cdot10^{-7}$	$6.0\cdot10^{-8}$-$6.5\cdot10^{-8}$	$3\cdot10^{-8}$-$5\cdot10^{-8}$
Arc 2	$5\cdot10^{-6}$-$1\cdot10^{-4}$		$4\cdot10^{-6}$-$4\cdot10^{-5}$
Arc 3	$5\cdot10^{-6}$-$5\cdot10^{-4}$	$1\cdot10^{-5}$-$2\cdot10^{-4}$	$3\cdot10^{-6}$-$3\cdot10^{-4}$
Arc 4	$5\cdot10^{-5}$-$2\cdot10^{-3}$	$2\cdot10^{-4}$-$2\cdot10^{-2}$	$2\cdot10^{-3}$-$4\cdot10^{-1}$
Arc 5		$2\cdot10^{-3}$-$5\cdot10^{-1}$	

Table 7. C_ω in 10% O_2 in the temperature range 300 °C – 500 °C (for Arc 1 only for 300 °C). The values are stated in F/cm^2.

	Blank	KNO_3 imp.	MnO_x imp.
Arc 1	$2\cdot10^{-7}$-$3\cdot10^{-7}$	$5.5\cdot10^{-8}$-$5.6\cdot10^{-8}$	$3\cdot10^{-8}$-$5\cdot10^{-8}$
Arc 2	$4\cdot10^{-6}$-$1\cdot10^{-5}$		$4\cdot10^{-6}$-$4\cdot10^{-5}$
Arc 3	$1\cdot10^{-4}$-$3\cdot10^{-4}$	$3\cdot10^{-5}$-$3\cdot10^{-4}$	$1\cdot10^{-5}$-$5\cdot10^{-4}$
Arc 4	$1\cdot10^{-3}$-$2\cdot10^{-3}$	$5\cdot10^{-4}$-$3\cdot10^{-3}$	$2\cdot10^{-4}$-$1\cdot10^{-2}$

Table 8. C_ω in 1000 ppm NO + 10% O_2 in the temperature range 300 °C – 500 °C (for Arc 1 only for 300 °C). The values are stated in F/cm^2.

	Blank	KNO_3 imp.	MnO_x imp.
Arc 1	$2\cdot10^{-7}$-$3\cdot10^{-7}$	$6.0\cdot10^{-8}$-$6.5\cdot10^{-8}$	$3\cdot10^{-8}$-$5\cdot10^{-8}$
Arc 2	$2\cdot10^{-6}$-$1\cdot10^{-5}$	$5\cdot10^{-7}$-$1\cdot10^{-4}$	$2\cdot10^{-6}$-$5\cdot10^{-5}$
Arc 3	$2\cdot10^{-5}$-$2\cdot10^{-4}$	$5\cdot10^{-6}$-$4\cdot10^{-4}$	$5\cdot10^{-6}$-$3\cdot10^{-4}$
Arc 4	$5\cdot10^{-5}$-$3\cdot10^{-3}$	$5\cdot10^{-4}$-$1\cdot10^{-3}$	$5\cdot10^{-5}$-$3\cdot10^{-4}$
Arc 5		$2\cdot10^{-3}$-$5\cdot10^{-1}$	

Table 9. The percentage difference in resistance between cells flushed in a 100 ml/min flow and 50 ml/min flow. A negative value states the resistance become lower in 50 ml/min flow compared to 100 ml/min flow.

	1000 ppm NO	10% O_2	1000 ppm NO + 10% O_2
Blank test			
Arc 2	3	0	-1
Arc 3	1	0	-2
Arc 4	-37	0	-8
KNO_3			
Arc 2		-5	0
Arc 3	-1	-2	0
Arc 4	-2	1	-5
Arc 5	-18		-7
MnO_x			
Arc 2	-9	-	
Arc 3	-15	-	2
Arc 4	-18	-	-5

Table 10. Resistance and C_ω during variations in the oxygen concentration. The data were recorded on one cell at 500 °C and the NO concentration was constant at 1000 ppm NO.

	Resistance [Ω cm^2]			C_ω [Ω/cm^2]		
	5% O_2	10% O_2	15% O_2	5% O_2	10% O_2	15% O_2
Arc2	35	34	34	$8.7 \cdot 10^{-6}$	$8.4 \cdot 10^{-6}$	$8.1 \cdot 10^{-6}$
Arc3	50	48	46	$1.4 \cdot 10^{-4}$	$1.4 \cdot 10^{-4}$	$1.4 \cdot 10^{-4}$
Arc4	65	48	40	$2.0 \cdot 10^{-3}$	$2.2 \cdot 10^{-3}$	$2.4 \cdot 10^{-3}$

Table 11. Resistance and C_ω during variations in the NO concentration. The data were recorded on one cell at 500 °C and the oxygen concentration was constant at 10% O_2.

	Resistance [Ω cm^2]			C_ω [Ω/cm^2]		
	500 ppm NO	1000 ppm NO	1500 ppm NO	500 ppm NO	1000 ppm NO	1500 ppm NO
Arc2	36	35	34	$4.0 \cdot 10^{-6}$	$8 \cdot 10^{-6}$	$7.6 \cdot 10^{-6}$
Arc3	47	46	44	$1.5 \cdot 10^{-4}$	$1.3 \cdot 10^{-4}$	$1.2 \cdot 10^{-4}$
Arc4	72	47	35	$1.7 \cdot 10^{-3}$	$2.3 \cdot 10^{-3}$	$2.9 \cdot 10^{-3}$

Table 12. Serial resistance and polarisation resistance in 1000 ppm NO + 10% O_2 in the beginning and the end of the tests. The values stated are the average values of the 3 or 4 cells tested in each test, and the number in the parenthesis state the uncertainties.

	Rs			Rp		
	Begin	End	Diff.	Begin	End	Diff.
	[Ωcm^2]	[Ωcm^2]	[%]	[Ωcm^2]	[Ωcm^2]	[%]
Blank	54(3)	57(3)	5	7635(911)	8460(689)	11
KNO_3 imp.	72(1)	64(3)	-11	4484(596)	6774(241)	51
MnO_x imp.	69(21)	212(101)	207	761(165)	11960(6193)	3650

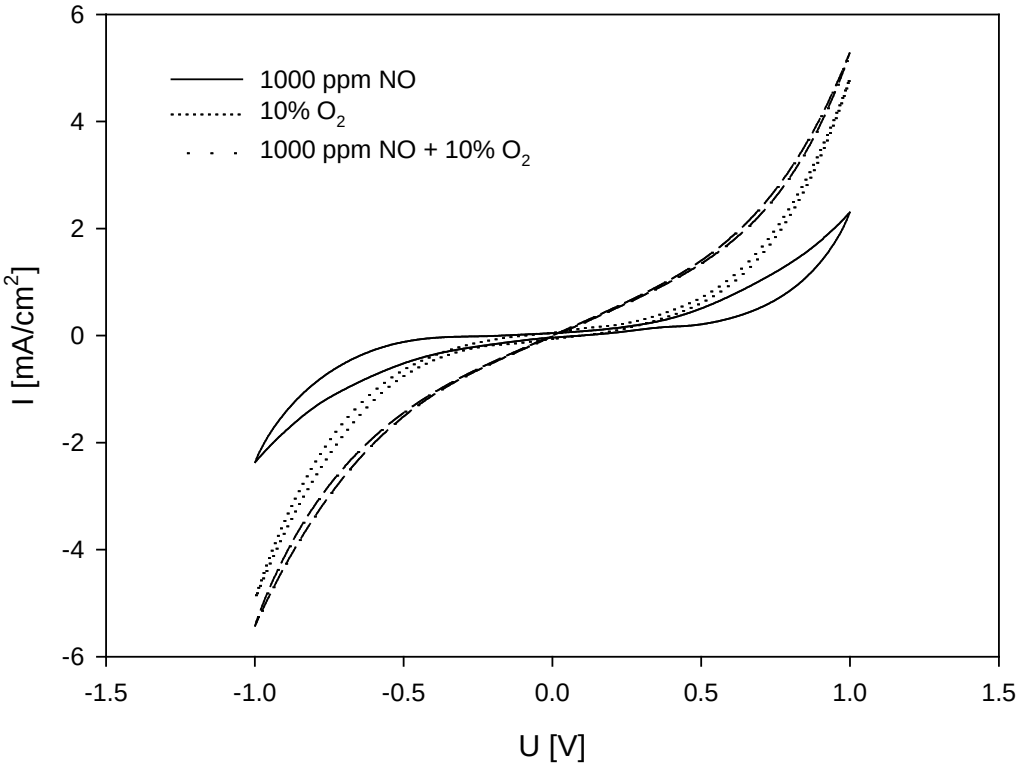
1000 ppm NO
10% O2
1000 ppm NO + 10% O2
I [mA/cm2]
U [V]
6
4
2
0
-2
-4
-6
-1.5
-1.0
-0.5
0.0
0.5
1.0
1.5

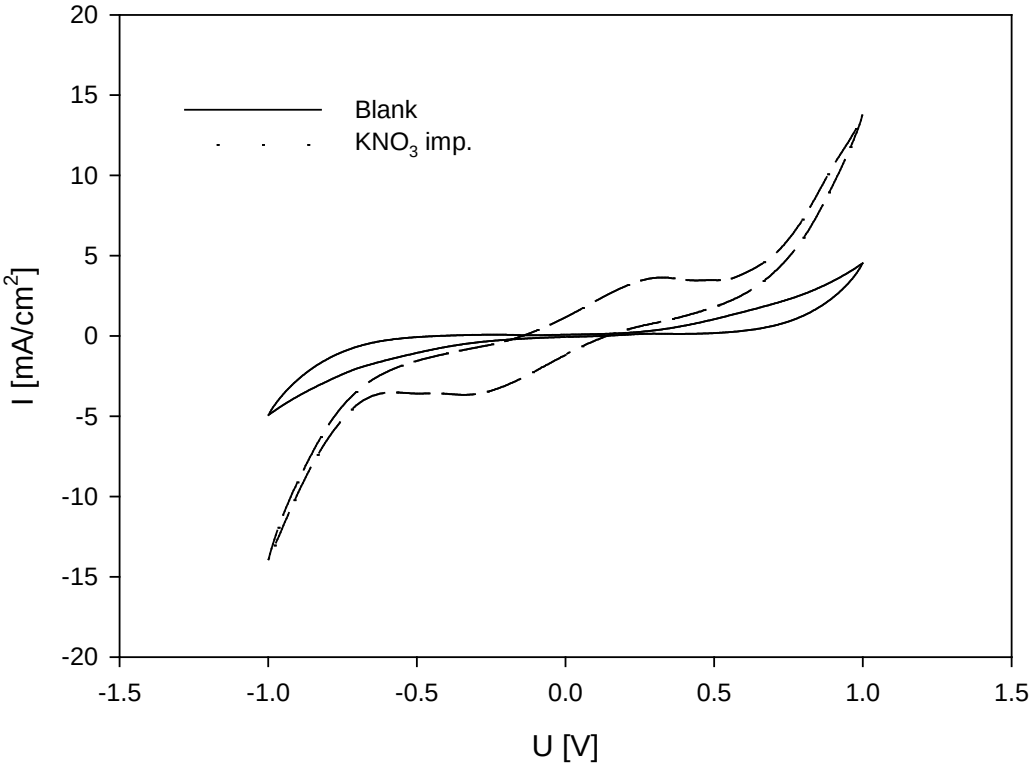
Blank
KNO3 imp.
I [mA/cm2]
U [V]
20
15
10
5
0
-5
-10
-15
-20
-1.5
-1.0
-0.5
0.0
0.5
1.0
1.5

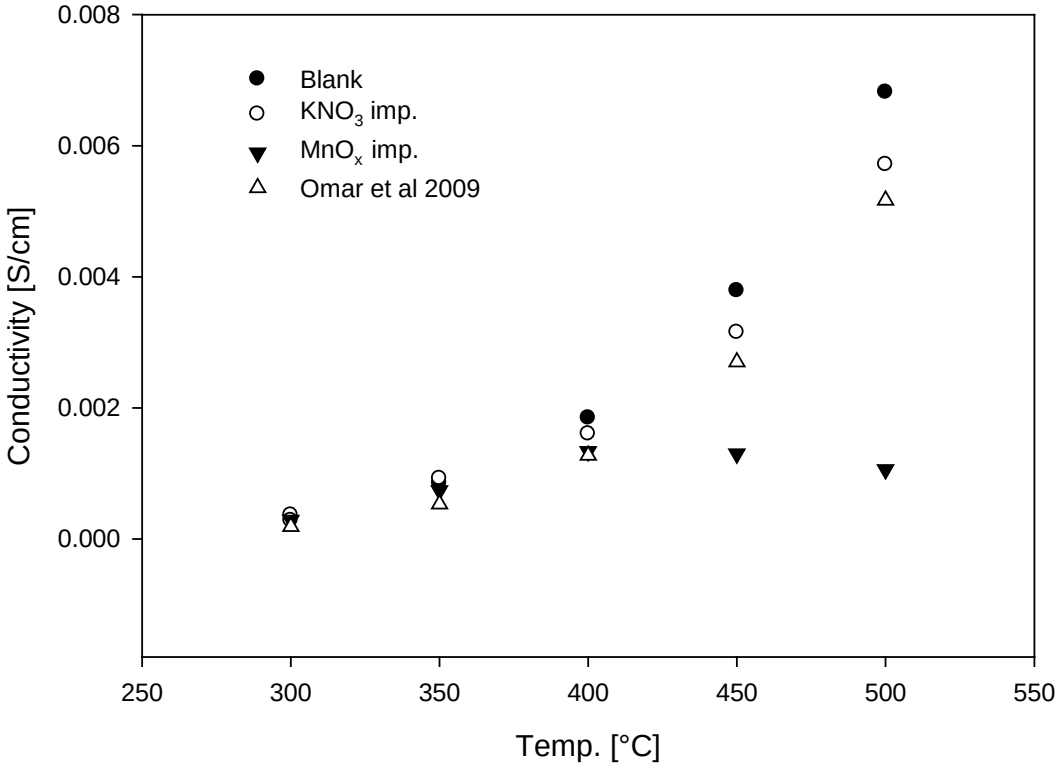
0.008
0.006
0.004
0.002
0.000
Conductivity [S/cm]
Blank
KNO3 imp.
MnOx imp.
Omar et al 2009
250
300
350
400
450
500
550
Temp. [°C]

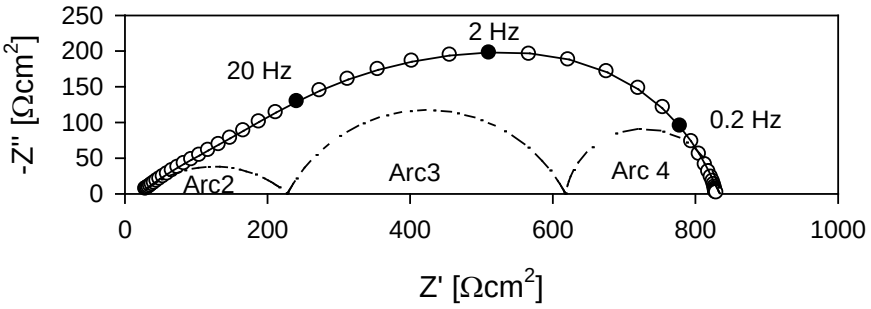
250
200
150
100
50
0
-Z'' [Ωcm2]
2 Hz
20 Hz
0.2 Hz
Arc2
Arc3
Arc 4
0
200
400
600
800
1000
Z' [Ωcm2]

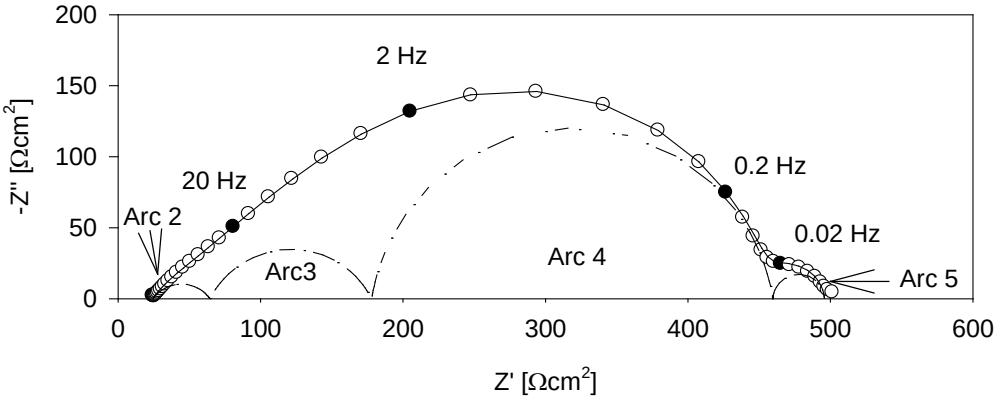
200
150
100
50
0
-Z'' [Ωcm2]
0
100
200
300
400
500
600
Z' [Ωcm2]
2 Hz
20 Hz
0.2 Hz
0.02 Hz
Arc 2
Arc3
Arc 4
Arc 5

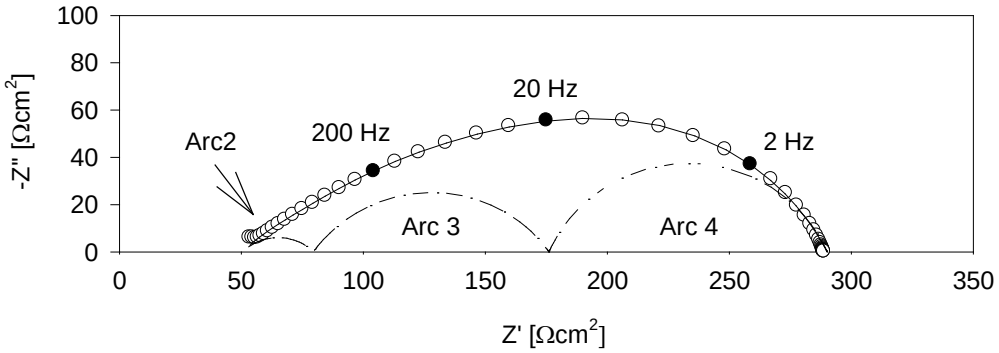
100
80
60
40
20
0
-Z'' [Ωcm2]
0
50
100
150
200
250
300
350
Z' [Ωcm2]
Arc2
200 Hz
20 Hz
2 Hz
Arc 3
Arc 4

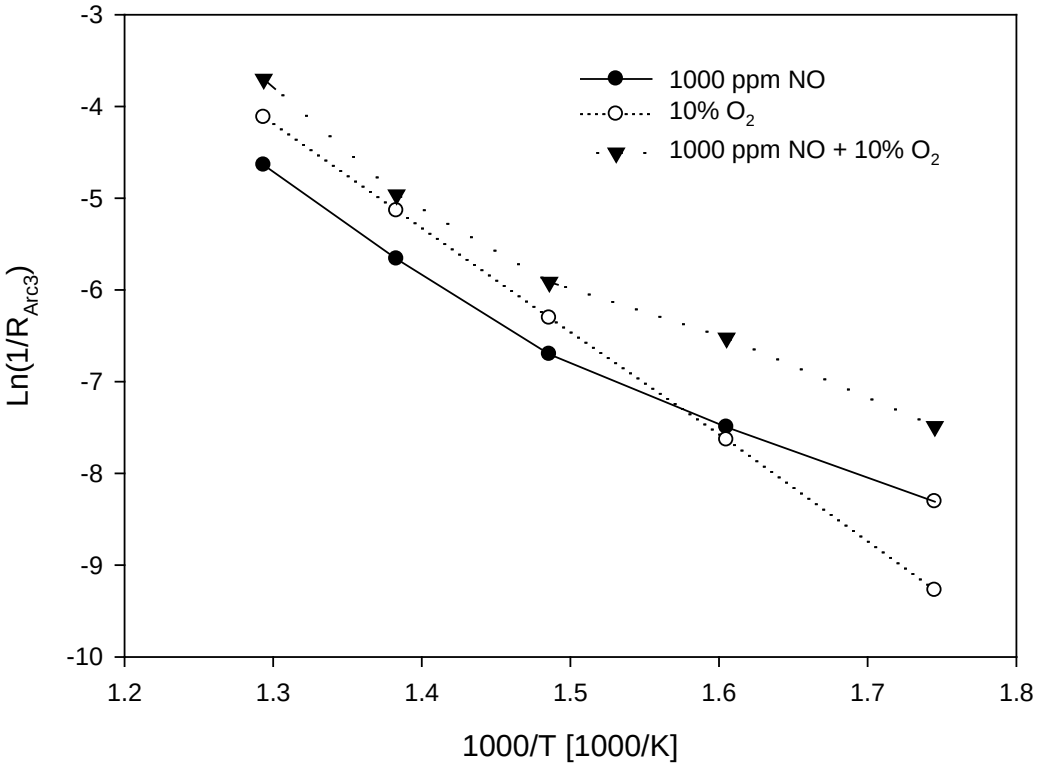
-3
-4
-5
-6
-7
-8
-9
-10
1.2
1.3
1.4
1.5
1.6
1.7
1.8
Ln(1/R_Arc3)
1000/T [1000/K]
1000 ppm NO
10% O2
1000 ppm NO + 10% O2

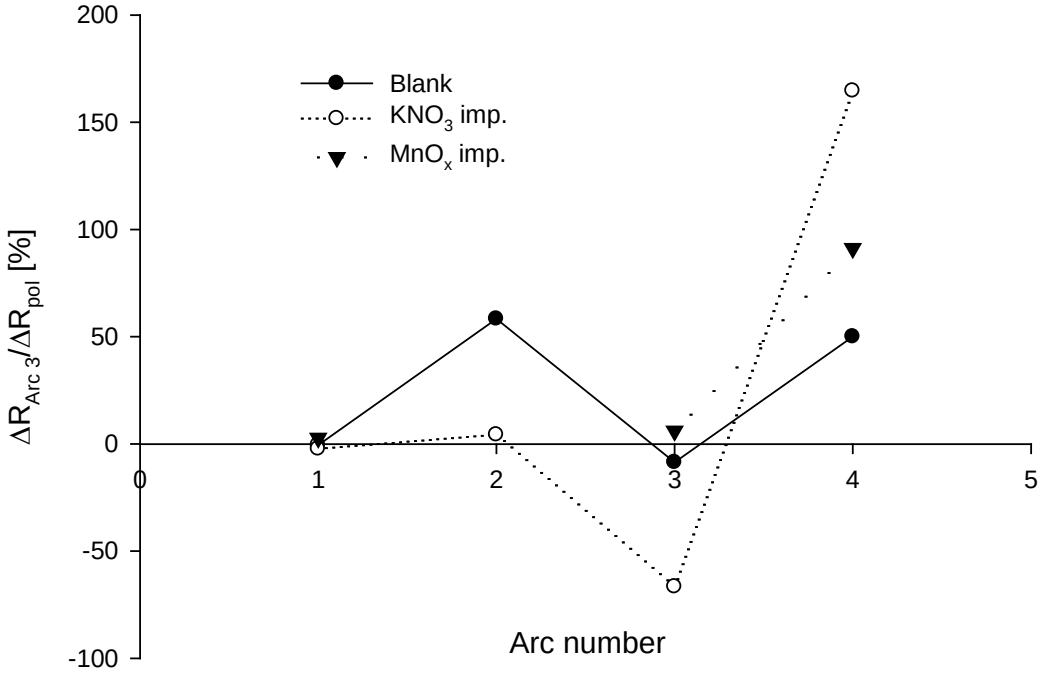
200
150
100
50
0
-50
-100
0
1
2
3
4
5
Blank
KNO3 imp.
MnOx imp.
ΔRArc 3/ΔRpol [%]
Arc number

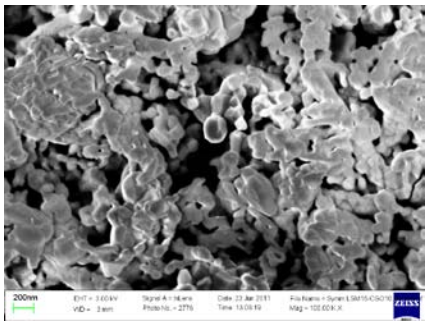

A1

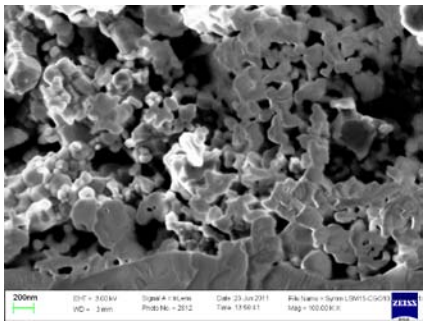

A2

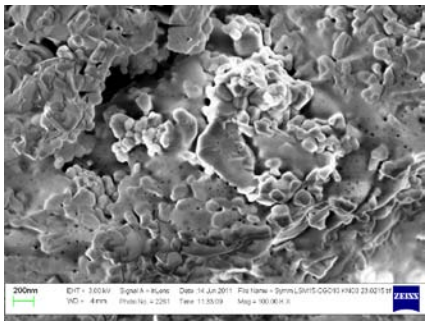

B1

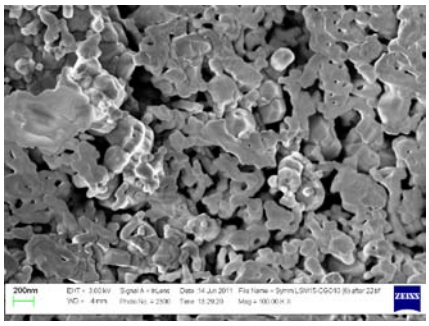

B2

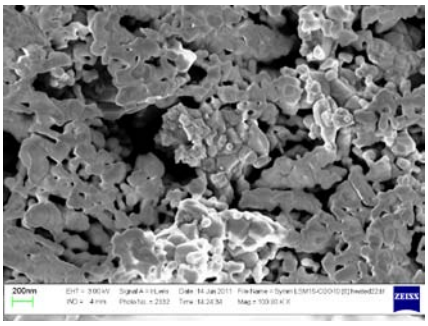

B3

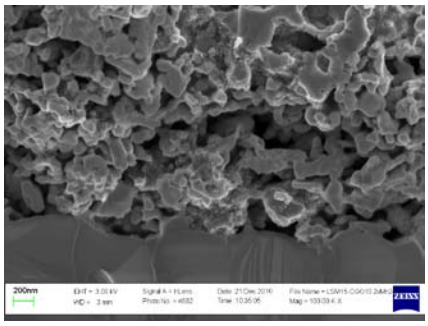

C1

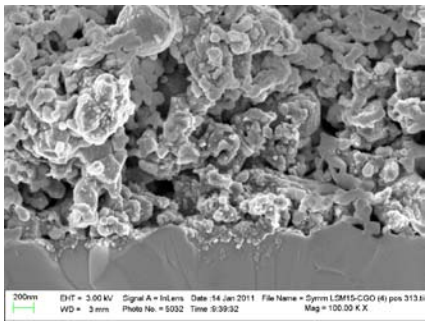

C2

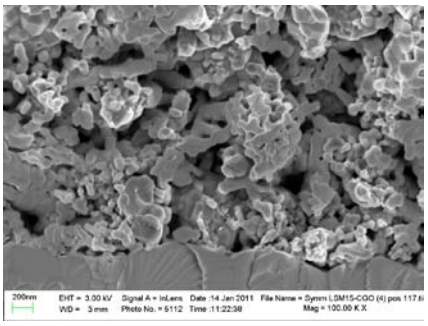

C3

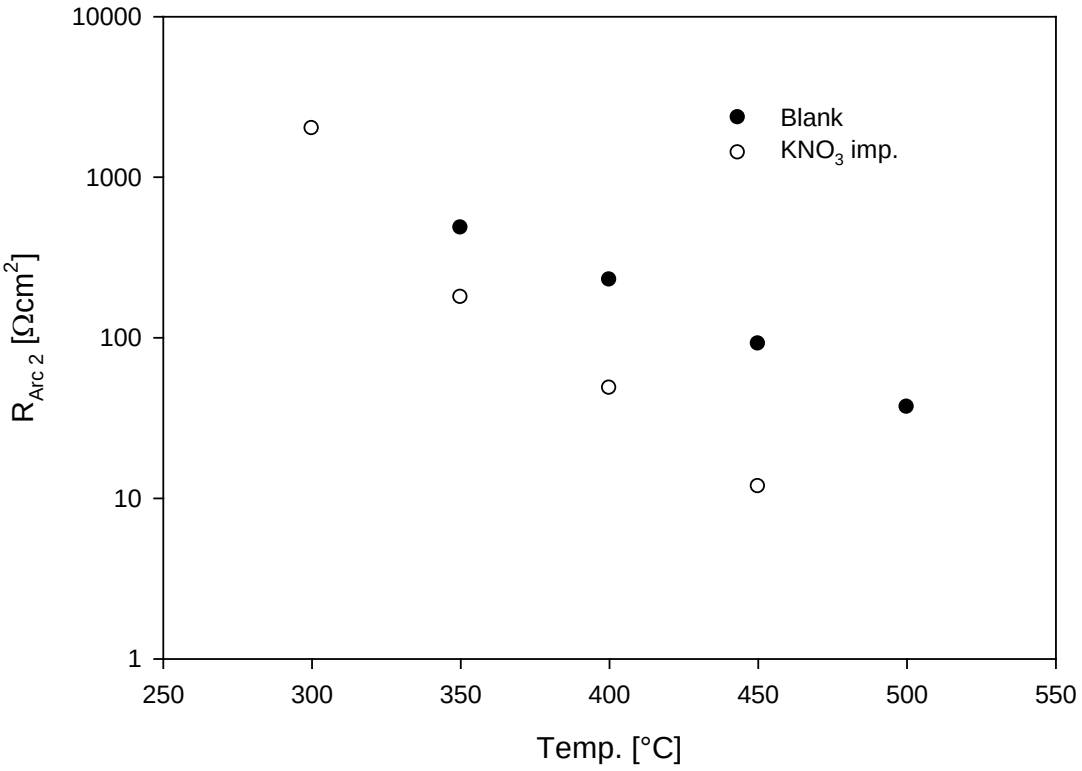
10000
1000
100
10
1
250
300
350
400
450
500
550
Temp. [°C]
$R_{Arc\,2}$ [Ωcm^2]
Blank
KNO_3 imp.

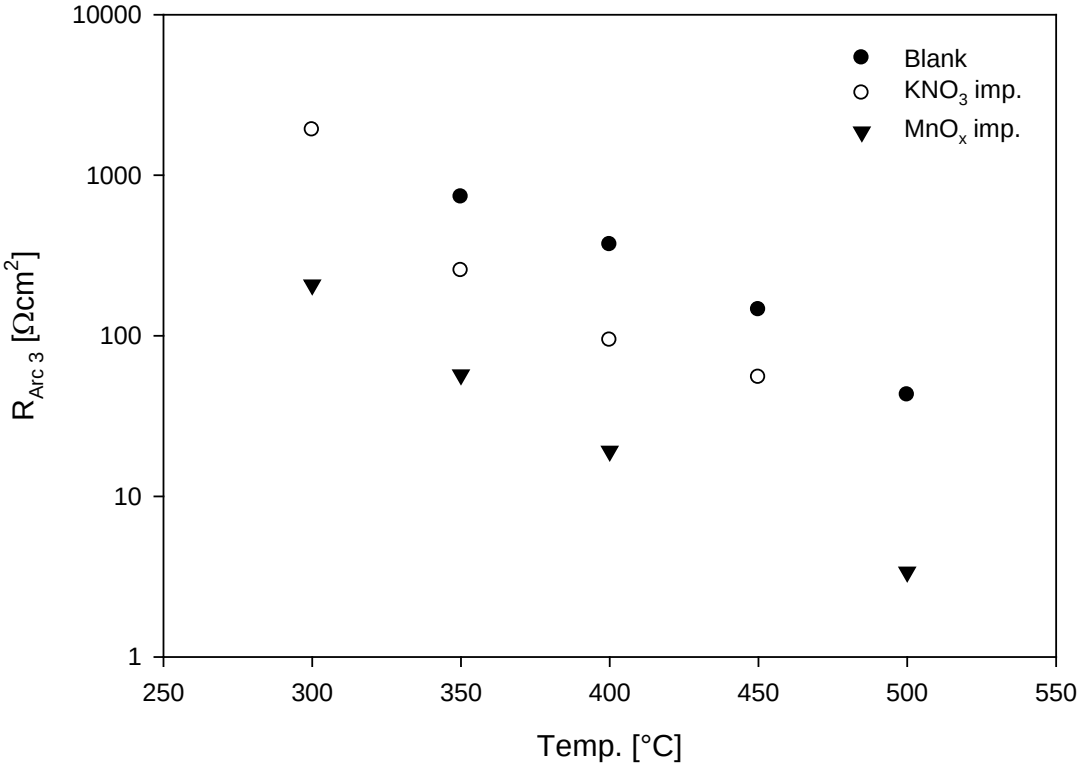
10000
1000
100
10
1
250
300
350
400
450
500
550
Temp. [°C]
$R_{Arc\ 3}$ [Ωcm^2]
Blank
KNO_3 imp.
MnO_x imp.

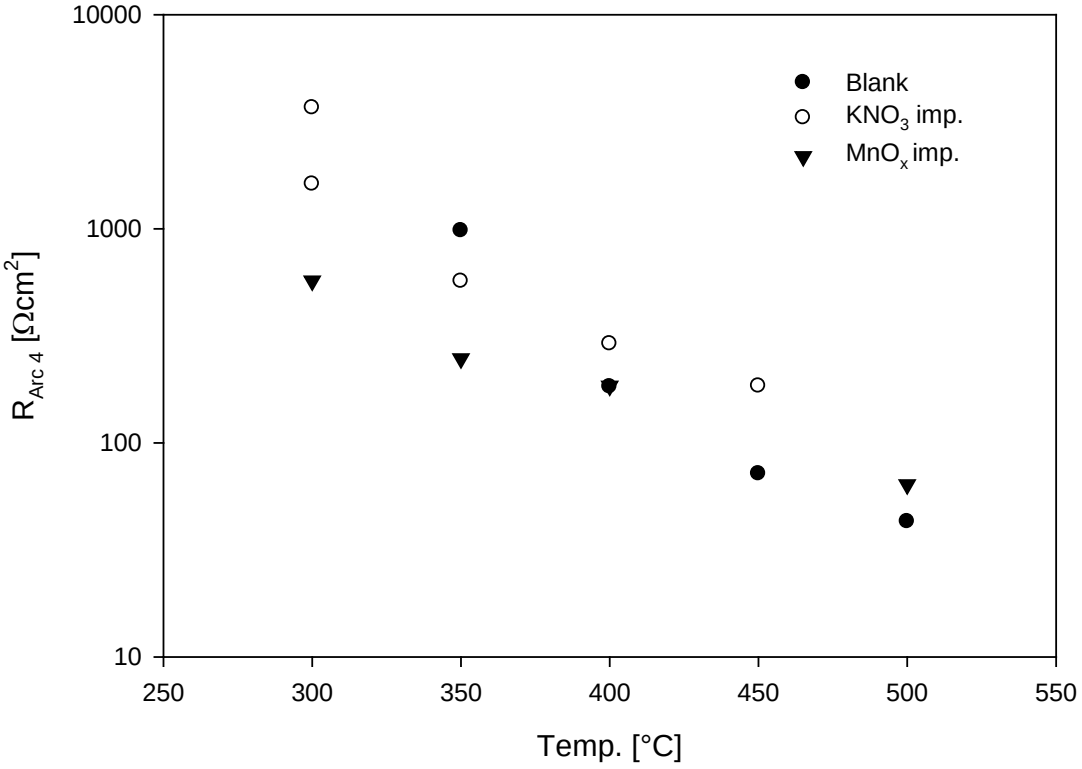
10000
1000
100
10
250
300
350
400
450
500
550
Temp. [°C]
$R_{Arc\ 4}$ [Ωcm^2]
Blank
KNO_3 imp.
MnO_x imp.

Figure 1. Cyclic voltammograms recorded on a blank LSM15-CGO10 symmetric cell in different atmospheres at 400 °C.

Figure 2. Cyclic voltammograms recorded at 450 °C in 1000 ppm NO on a LSM15-CGO10 cell without impregnation and impregnated with KNO_3.

Figure 3. Conductivity of the three tests with LSM15-CGO10 electrodes on CGO electrolyte compared to literature values for the conductivity of CGO.

Figure 4. Impedance spectrum recorded on cell without impregnation at 400 °C in 1000 ppm NO + 10% O_2. Black squares represents the experimental values, the red line is the fit and the three smaller were used for the deconvolution of the spectrum.

Figure 5. Impedance spectrum recorded on cell with KNO_3 impregnation at 400 °C in 1000 ppm NO + 10% O_2. Black squares represents the experimental values, the red line is the fit and the three smaller were used for the deconvolution of the spectrum.

Figure 6. Impedance spectrum recorded on cell with MnO_x impregnation at 400 °C in 1000 ppm NO + 10% O_2. Black squares represents the experimental values, the red line is the fit and the three smaller were used for the deconvolution of the spectrum.

Figure 7. Arrhenious plot of the arc3 resistance in 1000 ppm NO, 10% O2 and 1000 ppm NO + 10% O2. Note the apparent change in slope in the atmospheres containing NO.

Figure 8. Change in arc resistance relative to the entire change in polarisation resistance when spectra recorded at 300 °C in 1000 ppm + 10% O_2 at beginning and the end of the cell test are compared. Positive values state the arc increases in resistance, negative values the arc decreases in resistance.

Figure 9. SEM images of blank and impregnated LSM15-CGO10 electrodes before testing, after testing and after heat-treatment as the tested cells. The images show A1: Blank electrode before testing, A2: Blank electrode after testing, B1: KNO_3 impregnated electrode before testing, B2: KNO_3 impregnated electrode after testing, B3: KNO_3 impregnated electrode after heat treatment, C1: MnO_x impregnated electrode before testing, C2: MnO_x impregnated electrode after testing, C3: MnO_x impregnated electrode after heat

Figure 10. Resistance of arc 2 in 1000 ppm NO + 10% O_2.

Figure 11. Resistance of arc 3 in 1000 ppm NO + 10% O_2.

Figure 12. Resistance of arc 4 in 1000 ppm NO + 10% O_2.